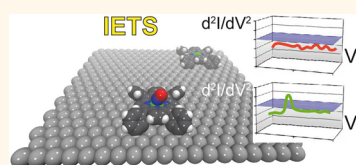


# Probing Nitrosyl Ligation of Surface-Confining Metalloporphyrins by Inelastic Electron Tunneling Spectroscopy

Shiri R. Burema,<sup>†</sup> Knud Seufert,<sup>‡</sup> Willi Auwärter,<sup>‡</sup> Johannes V. Barth,<sup>‡</sup> and Marie-Laure Bocquet<sup>†,\*</sup>

<sup>†</sup>Laboratoire de Chimie, CNRS UMR 5182, Ecole Normale Supérieure de Lyon, 46 Allée d'Italie, 69364 CEDEX07 Lyon, France, and <sup>‡</sup>Physik Department E20, Technische Universität München, James-Franck Str. D-85748 Garching, Germany

**ABSTRACT** Complexes obtained by the ligation of nitric oxide (NO) to metalloporphyrins represent important model systems with biological relevance. Herein we report a molecular-level investigation of surface-confined cobalt tetraphenyl porphyrin (Co-TPP) species and their interaction with NO under ultrahigh vacuum conditions. It is demonstrated that individual NO adducts can be desorbed using the atomically sharp tip of a scanning tunneling microscope, whereby a writing process is implemented for fully saturated regular metalloporphyrin arrays. The low-energy vibrational characteristics of individual Co-TPP-nitrosyl complexes probed by inelastic electron tunneling spectroscopy (IETS) reveal a prominent signature at an energy of  $\approx 31$  meV. Using density functional theory-based IETS simulations—the first to be performed on such an extensive interfacial nanosystem—we succeed to reproduce the low-frequency spectrum for the NO-ligated complex and explain the absence of IETS activity for bare Co-TPP. Moreover, we can conclusively assign the IETS peak of NO-Co-TPP to a unique vibration mode involving the NO complexation site, namely, the in-plane Co—N—O rocking mode. In addition, we verify that the propensity rules previously designed on small aromatic systems and molecular fragments hold true for a metal—organic entity. This work notably permits one to envisage IETS spectroscopy as a sensitive tool to chemically characterize hybrid interfaces formed by complex metal—organic units and gaseous adducts.



**KEYWORDS:** porphyrin · Ag(111) · NO · STM · inelastic electron tunneling spectroscopy · DFT

The interactions of metalloporphyrins with diatomic molecular species are the heart of many key biological concepts since metalloporphyrins are toy models for heme proteins forming myoglobin and hemoglobin. An important question is how a metalloporphyrin discriminates among the isosteric  $\pi$ -accepting carbonyl CO, nitrosyl NO, and dioxygen O<sub>2</sub> ligands. Consequently, the metalloporphyrin–ligand interactions captured the interest of chemists and theoreticians early on.<sup>1</sup> Among them, the metalloporphyrin–nitrosyl complexes have been studied intensively since NO has emerged as a ubiquitous signaling molecule in biology<sup>2,3</sup> after being longly considered as a pollutant and poison. Special attention focuses on vibrational features as fingerprints for interactions of the complex with its environment.<sup>4–6</sup> The studies considered not only the gas phase, the solution,<sup>2,7</sup> and the solid state<sup>8,9</sup> but in recent years also nitrosyl complexes immobilized on supports like inert metal surfaces.<sup>6,10–12</sup> Without

exception in iron(II) and cobalt(II) metalloporphyrins, the NO is coordinated in a bent apical fashion, and this ligation motive is preserved in all disordered or ordered phases. Although not studied as much as their iron analogues, cobalt porphyrins gained prominent attention for the binding and activation of NO. In particular, the Co-TPP-NO (Co-TPP = cobalt tetraphenyl porphyrin) has been explored as an isolectronic model for oxygenated protoheme.<sup>13</sup> On Ag(111), nonligated Co-TPPs assemble into large well-ordered islands even at submonolayer coverage as probed by scanning tunneling microscopy (STM). The molecules show a nonplanar conformation upon adsorption, the so-called saddle-shape deformation: one pair of opposing pyrroles is bent upward ( $\alpha$ -pyr) with respect to the molecular plane, while the other pair is bent downward ( $\kappa$ -pyr) and the four phenyl meso-substituents are rotated.<sup>14–16</sup> By using XPS, evidence of electron transfer from the silver surface to the Co metal center of Co-TPP was obtained.<sup>10,17</sup>

\* Address correspondence to mbocquet@ens-lyon.fr.

Received for review March 2, 2013  
and accepted May 29, 2013.

Published online May 29, 2013  
10.1021/nn401058z

© 2013 American Chemical Society

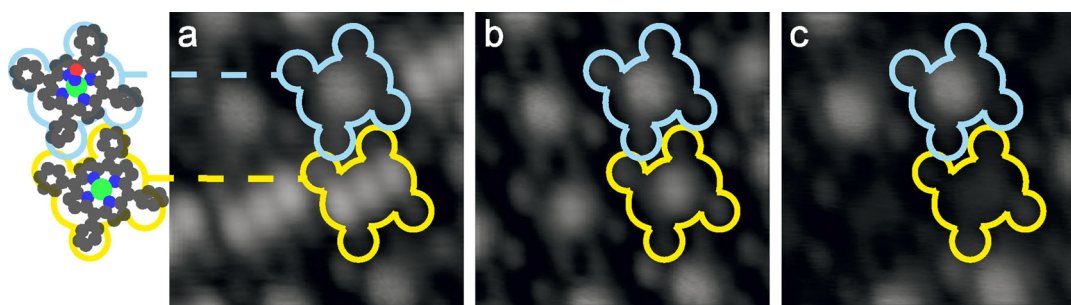


**Figure 1.** Sequence of STM topographs of the same area imaged at different sample biases. One of the bare Co-TPPs is outlined in yellow in each image. (a) Three bright maxima represent the main axis of the molecule. In contrast, NO-Co-TPP (blue) shows only one central protrusion, while the peripheral features are unchanged. A contrast inversion is observable from (a) ( $-700$  mV,  $55$  pA) to (c) ( $300$  mV,  $55$  pA). The molecules may be almost indistinguishable at intermediate voltages (b) ( $-300$  mV,  $55$  pA). At the energy of the Co-TPP HOMO, the nonligated porphyrin appears brighter (a), while in the unoccupied energy region at positive sample bias, this contrast is inverted (c).

The authors also showed that the above-mentioned Co–Ag interaction is suppressed after axial coordination of NO to the cobalt porphyrin and suggested that this effect results from competition between the two axial ligands (NO and the silver surface, considered as a point ligand). Furthermore, on a thin film of Ni(001), nitrosyl ligation can even influence the magnetic properties of Co-TPP via a spin switch.<sup>18</sup>

In this work, we investigated bond-breaking and vibrational characteristics of the nitrosyl ligation. First, the process of controlled removal of NO ligand is demonstrated using the STM tip as a writing tool. Second, inelastic electron tunneling spectroscopy (IETS) with the STM is used as a technique for the identification of nitrosyl ligation. Traditionally, IETS yields insight into the vibrational fingerprint of adsorbed molecules *via* the excitation of modes by tunneling electrons from the STM tip that match the  $\hbar\omega$  energy.<sup>19–24</sup> Despite the technical difficulty and the ongoing investigation of the selection rules, the IETS technique has previously been applied successfully for the discrimination of subtle adsorbate features that are unaccessible by conventional STM imaging like denticity,<sup>25</sup> hybridization,<sup>26,27</sup> orientations,<sup>28,29</sup> chemical nature,<sup>29,30</sup> and structural isometry.<sup>31</sup>

As a main finding, the presented IETS measurements evidence a unique signal at a sample bias voltage of about  $31$  mV for the NO-ligated Co-TPP, while no inelastic signal can be detected on the bare porphyrin. By means of extremely large *ab initio* IETS simulations, we reproduce the experimental measurements for both ligated and nonligated Co-TPP molecules, permitting identification of the unique active vibration of the NO-ligated Co-TPP to be a Co–N–O in-plane rocking mode. This difference in IETS response between the NO-ligated and nonligated Co-TPP species not only enables their discrimination but also opens a route for applications as toxic gas nanosensors, nano-switches, nanotracing of gas transport etc. From a fundamental point of view, the presented IETS simulations extend the previously postulated selection rules<sup>25,29,31–38</sup>

that were derived for much smaller adsorbed aromatic systems.

## EXPERIMENTAL RESULTS

On the basis of both the high mobility of Co-TPP on Ag(111) at room temperature and the attractive intermolecular forces *via* the so-called T-type interaction between their *meso*-substituents, the porphyrins assemble into large highly ordered islands even at coverages well below one monolayer. Auwärter *et al.*<sup>14</sup> observed a noncommensurate Co-TPP assembly with three possible azimuthal orientations of the molecules each representing a parallel alignment of the main axis with the  $\langle 1\bar{1}\bar{2} \rangle$  high-symmetry direction of the substrate. Thereby, the main axis of a bare Co-TPP is represented by three maxima (see Figure 1a outlined in yellow). The central protrusion can be assigned to the metal Co ion and the outer ones to the two opposite upward bent pyrrole rings, the  $\alpha$ -pyrs. The four dimer peripheral features represent the four phenyl substituents responsible for the attractive interaction. This two-fold symmetry is related to the molecular saddle-shape deformation where not only the macrocycle is distorted but also the substituents are rotated with respect to the molecular plane. While this conformation was found to be important for the ligation with CO *via* a *cis*-carbonyl geometry,<sup>11,15</sup> NO binds directly to the metal center as generally expected. As reported recently, this NO coordination to the metal center affects not only the appearance of Co-TPP in STM images but also the electronic structure.<sup>11,39</sup> The former two-fold symmetry of the molecular core is strongly reduced, and the molecule shows one central protrusion (see Figure 1a outlined in blue). Figure 1 shows an image sequence of bare (yellow) and ligated (blue) Co-TPPs. It is obvious that the overall DOS at  $-700$  mV sample bias voltage, probing the highest occupied molecular orbital (HOMO) of the bare Co-TPP, is different for the two molecules. As a result of the quenching of the HOMO, the ligation with NO leads to a dimer and a more four-fold symmetric appearance

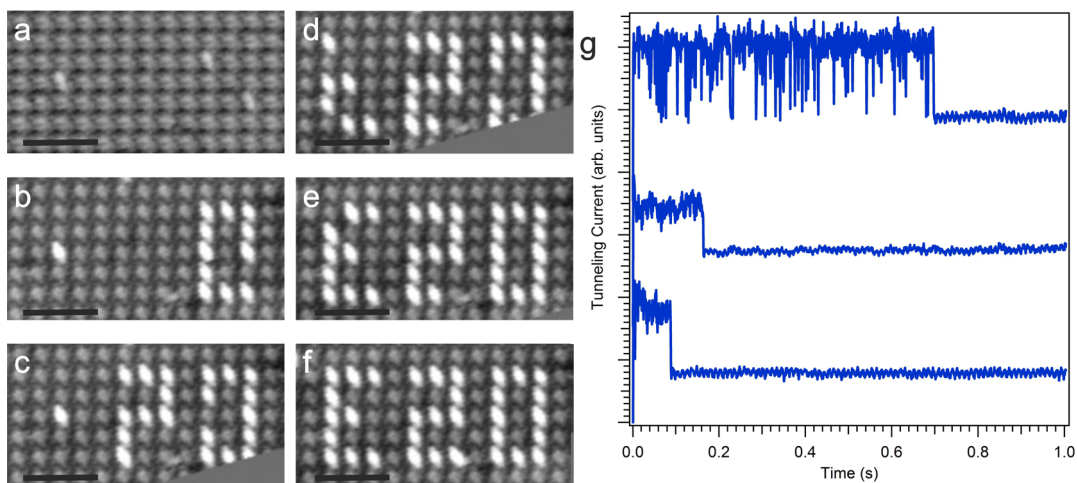


**Figure 2.** Series of STM images of the same area during a writing process (a–f). A Co-TPP island on Ag(111) fully saturated with NO (gray features) can be used as a template by NO abstraction. Positioning the tip over a molecule and setting a sample bias voltage of 800 mV leads to controlled desorption of the NO (white features). Repeating this procedure at different molecules allows writing on a molecular level. (g) Some  $I(t)$  traces of such desorption processes. A step to a different conductance indicates the moment of the desorption (image parameters: (a–f)  $-684$  mV,  $77$  pA; scale bar is  $50$  Å; (g) stabilization parameters:  $800$  mV,  $77$  pA).

(Figure 1a). Reducing the bias to  $-300$  mV yields a similarity of both molecules (Figure 1b). A reversal of the polarity of the sample bias results in an inversion of the topographic contrast. The imaging of NO-Co-TPP is nearly unaffected, while the macrocycle of the bare porphyrin is less pronounced (Figure 1c). It should be noted that the apparent height difference between bare and ligated Co-TPP can vary with the tip termination.<sup>11</sup> Compared to Figure 2, the high-resolution images in Figure 1, presumably originating from an NO modified tip, evidence a more subtle height difference. Nevertheless, the relative contrast does not depend on the tip termination but sensitively on the bias voltage.

The moderate bond of NO to the Co-TPP can efficiently be broken *via* voltage pulses applied by the STM tip. On the one hand, the low stability of the nitrosyl binding to the Co ion limits the observation of the high-energy electronic structure, but on the other hand, it enables the controlled desorption of single nitrosyl ligands *via* STM manipulation. Once the tip is centered above a NO-Co-TPP, the feedback loop is opened at a set point current of  $77$  pA and a sample bias of  $800$  mV. In the recorded  $I(t)$  traces displayed in Figure 2g, a steplike change of the conductance is observed after a given time, which is assigned to the desorption of the NO. The lower current level after the desorption is consistent with topographic images at this bias. Repeating this procedure on the very same molecule leads to no additional changes in the current level. After the bias pulse, the molecule appears brighter in STM images recorded at negative sample bias and generally looks identical to bare Co-TPP. With this method, it is possible to write on a molecular level whereby the ligated porphyrins on Ag(111), assembled into large well-ordered islands with a square unit cell,

act as a template. Figure 2 shows an image sequence of such a writing process. After several manipulations, a topograph is taken at the energy of the HOMO resonance of Co-TPP to check the desorption. The sequence in Figure 2a–f is done within  $15$  min and shows the letters E 20, representing the name of the chair at the Technische Universität München. As it can be deduced from Figure 2g, the actual writing process only takes seconds at these parameters. Using higher sample bias voltages, it is possible to remove the NO in large areas up to several hundreds of square nanometers. This nonlocal desorption points to a field-enhanced process.<sup>40</sup> Based on the available data, the interference of another mechanism such as surface-mediated electron propagation recently reported on semiconductor substrates cannot be excluded.<sup>41</sup>

Accordingly, the electronic structure of NO-Co-TPP at energies exceeding approximately  $800$  meV is not accessible by scanning tunneling spectroscopy (STS). However, to get a closer insight into the system, IETS can be used to look at the vibrational fingerprint of NO-Co-TPP on Ag(111). To this end, the STM tip is positioned above the center of a NO-Co-TPP molecule, the feedback is switched off, and  $d^2I/dV^2$  spectra are recorded. This procedure is repeated with the very same tip on a bare Co-TPP, and the difference of both spectra is analyzed (see Figure 3). The signal on the ligated molecule shows a prominent peak around at  $30.6$  meV and a dip at  $-31.7$  meV. The symmetric behavior of both the energy position with respect to the Fermi level and the intensity clearly points to a vibronic excitation as the origin of these spectral features.<sup>23,42</sup> In addition, reference spectra recorded under identical conditions on bare Co-TPP species do

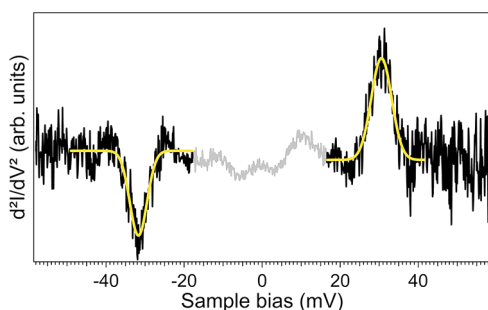


**Figure 3.** Inelastic electron tunneling spectra of NO-Co-TPP adsorbed on Ag(111) between 0 and  $\pm 60$  mV. The  $d^2/dV^2$  signal shown here is difference of the sum of 20 spectra taken on a bare Co-TPP (noisy silent signal) and on NO-Co-TPP. A clear vibrational signal is visible at an energy of about 31 meV. The dip and the peak are fitted with a single Gauss distribution.

not show these vibrational signals (see Supporting Information). Spectra repeatedly recorded on different NO adducts and porphyrins evidence that this signal is only detected on NO-Co-TPP species. Although the inelastic signal was detected also at slightly off-center positions, no systematic IETS mapping experiments were performed. Thus, we conclude that the inelastic signal corresponding to an excitation energy of about 31 meV is related to the ligation of the porphyrin with NO. Based solely on our experiments, an unambiguous assignment of the observed excitation to an unique vibration mode of the complex is not feasible. Therefore, extensive calculations of IETS spectra are required, although these are really challenging being a computationally very demanding task, never achieved so far. The theoretical results are discussed in the following section.

## THEORETICAL RESULTS

As illustrated in Figure 4, NO-Co-TPP exhibits a saddle-shape conformation in its favored adsorption position on the bridge site of a Ag(111) surface. This saddling is similar to the nonligated case (not shown) and the  $(CO)_2$ -Co-TPP case on Cu(111).<sup>15</sup> For the bare case, the bonding distance between Co and Ag surface atoms is 2.8 Å. When NO ligates in a monodentate way, it induces a vertical lifting of the Co atom, as illustrated in Figure 4, which consequently weakens the central bond between the Co and Ag atoms at 3.5 Å. This effect is referred to as the trans-labilizing effect of NO recalled in the introduction.<sup>2</sup> As expected for diatomic gases, NO binds the adsorbed cobalt porphyrin in a bent apical fashion with a Co–N–O angle of  $120^\circ$  and no tilt angle. This coordination geometry is fully consistent with the so-called Enemark–Feltham count rule of  $n = 8$  (summing the d electrons of Co(II) and the electron of the NO  $\pi^*$  orbital<sup>2</sup>) and permits optimization of the orbital interaction between the NO  $\pi^*$  orbital lying in the normal plane of the surface and the Co  $d_{z^2}$  orbital, illustrated in Figure 5. The chemical

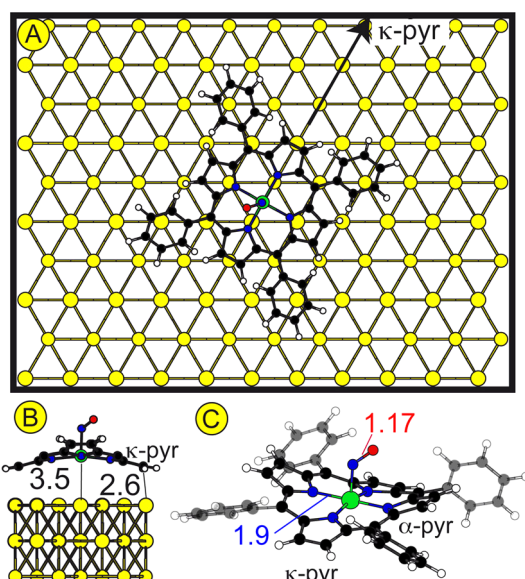


**Figure 4.** Atomistic models obtained from DFT calculations where Co-TPP is placed over the bridge site of Ag(111) with the  $\kappa$ -pyr groups aligned with the dense packed rows. (A) Top view of the  $p(11 \times 5\sqrt{3})$  rectangular unit cell considered in the DFT calculation. (B) Side zoom-in view of (A) with key bonding distances in Å where the phenyl substituents are removed for clarity. (C) Perspective view of the ligated porphyrin where the substrate has been removed and the phenyl substituents are shaded for clarity.

interaction with NO results in a significant downshift in energy of the  $Co\ d_{z^2}$  orbital, which is responsible for the STM contrast at the center of the nonligated complex. Furthermore, the comparative PDOS plots of bare and NO-ligated porphyrins projected on the molecular orbitals (MO) of the substrate-free porphyrins permit selection of the prominent tunneling-active states (see Supporting Information). As a result, the HOMO states seem to dominate the STM contrast at  $-0.7$  V. Since the ligated HOMO state peaks at  $-1$  eV, lying  $0.2$ – $0.3$  eV lower than the nonligated HOMO state, this may explain the reduced apparent height of ligated species at this specific negative bias. However the DOS-related and spatial arguments of the MO-derived states detailed in Supporting Information are not enough to fully rationalize the bias-dependent contrast reversal observed in Figure 1. Indeed, the bent position is neither static nor rigid: as proved by NMR<sup>8</sup> and X-ray diffraction<sup>9</sup> conducted on Co-TPP-NO in the solid state, NO is swinging over four equivalent positions on one side of the porphyrin plane. The dynamic move of the nitrosyl ligand makes it difficult to compare the measured STM images to STM simulations (not shown) that only consider one static configuration.

After having optimized the interfacial structure, one needs to perform a vibrational analysis to obtain insight into the possible active vibrations in IETS. In the following analysis, the IET signals simulated for the lowest and highest frequency modes of the adsorbate can be discarded due to the absence of (noise-free)

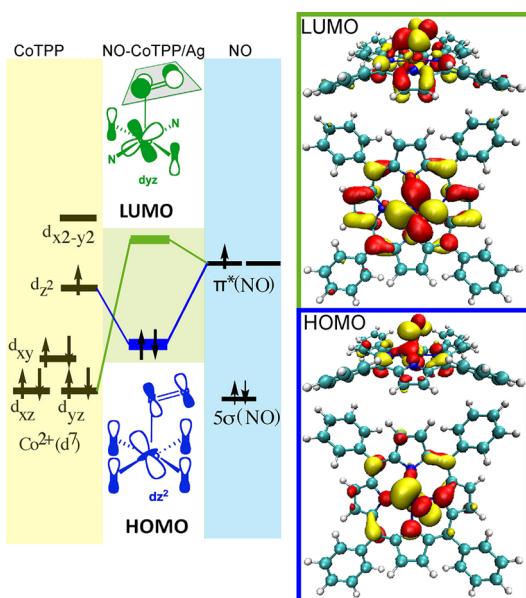


**Figure 5.** Simplistic molecular orbital (MO) diagram displaying the binding interaction between the frontier orbitals of NO and the d orbitals of the cobalt atom in the porphyrin structure as adsorbed on the metal surface. Because of the suppression of a surface-to-porphyrin charge donation after NO coordination, the electronic structure of adsorbed NO-Co-TPP is approximated by an isolated porphyrin species. This gives rise to the frontier orbitals of NO-Co-TPP, represented schematically (left panel, side view) and by means of *ab initio* calculations (right panel, side and top views).

experimental data in these regions. As explained in the methodology section, the vibrational modes for the adsorbed porphyrin sketched in Figure 7 have only been considered in the inner ring approximation of the adsorbed porphyrin, which consists of moving only the NO- $\text{CoN}_4$  subunit while the rest of porphyrin is kept rigid (model A in Figure 6). In order to quantify the error made in the frequency values calculated within this model, the vibrations within two other models (labeled B and C in Figure 6) have been calculated. When comparing the frequency values between model A and model B, the adsorption effect is accounted for. Accordingly, when comparing model C and model B, the inner ring effect is quantified in the gas phase. From Table 1, the adsorption effect costs about  $\pm 2$  meV, while the inner ring effect is not homogeneous among the frequencies, although it remains limited to  $\pm 1\text{--}2$  meV. In total, our approximation (model A) yields an error of  $\pm 1\text{--}4$  meV, which is smaller than the intrinsic errors arising from the choice of the DFT functionals. Moreover, the IETS signal is only detected in the close vicinity of the molecule center. Hence, our model is meaningful for the subsequent comparison between experimental and simulated IETS spectra, and the error bar is expected to range about a few meV.

In Figure 7, we show the IETS activities per vibration mode calculated in % efficiency at the center of the adsorbate for the NO-ligated Co-TPP (a) and the bare

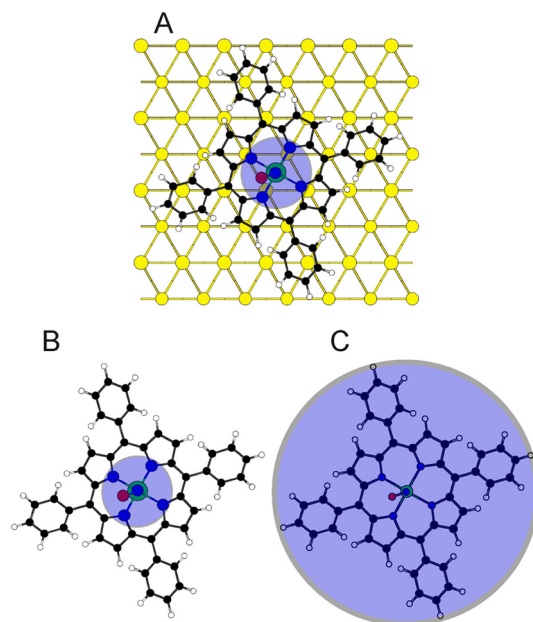


**Figure 6.** Illustration of the three levels of vibrational analysis described in Table 1: (A) adsorbed, ring; (B) isolated, ring; and (C) isolated, total. The adsorbate atoms that are included in the calculations of the normal modes are shaded blue. Model A corresponds to the relaxation of the inner porphyrin ring ( $\text{NO}-\text{CoN}_4$  part), while being adsorbed on the  $\text{Ag}(111)$  surface; model B to the similar subunit in the gas phase; and model C to an entire relaxation of the ligated porphyrin structure in the gas phase.

Co-TPP (b) species adsorbed on  $\text{Ag}(111)$ . We first discuss the simulated IETS signature of the NO-Co-TPP adsorbate. Ten vibrations were computed in the experimentally accessed region (roughly below 60 meV) and are sketched in Figure 7. Only three of them yield a measurable inelastic signal marked with colors and involve the frequencies of 10, 13, and 37 meV. Two of these modes belong to translational motions of NO, which are intrinsically coupled to surface phonons due to their manifestation in the low-energy region (*i.e.*, 10 and 13 meV). The other active normal mode corresponds to a Co–N–O in-plane rocking vibration at 37 meV. At first sight, there seem to be some discrepancies between the calculated (Figure 7) and measured (Figure 3) IET spectra. The low-energy modes (10 and 13 meV) have not been detected experimentally. However, the calculated IET signals of these two frustrated translation (FT) modes are not reliable because in reality they may be polluted by the coupling to other modes within the same energy window (*i.e.*, low-frequency modes of the rest of the porphyrin atoms and metallic phonons). A valuable comparison between the IETS experiments and theory within this energy window below 20 meV is not yet possible also because the measurements in this region suffer from spurious noise contributions (see the raw data in Supporting Information). This is the reason why the IETS spectrum presented in Figure 3 is a difference spectrum between the bare and NO-ligated species:

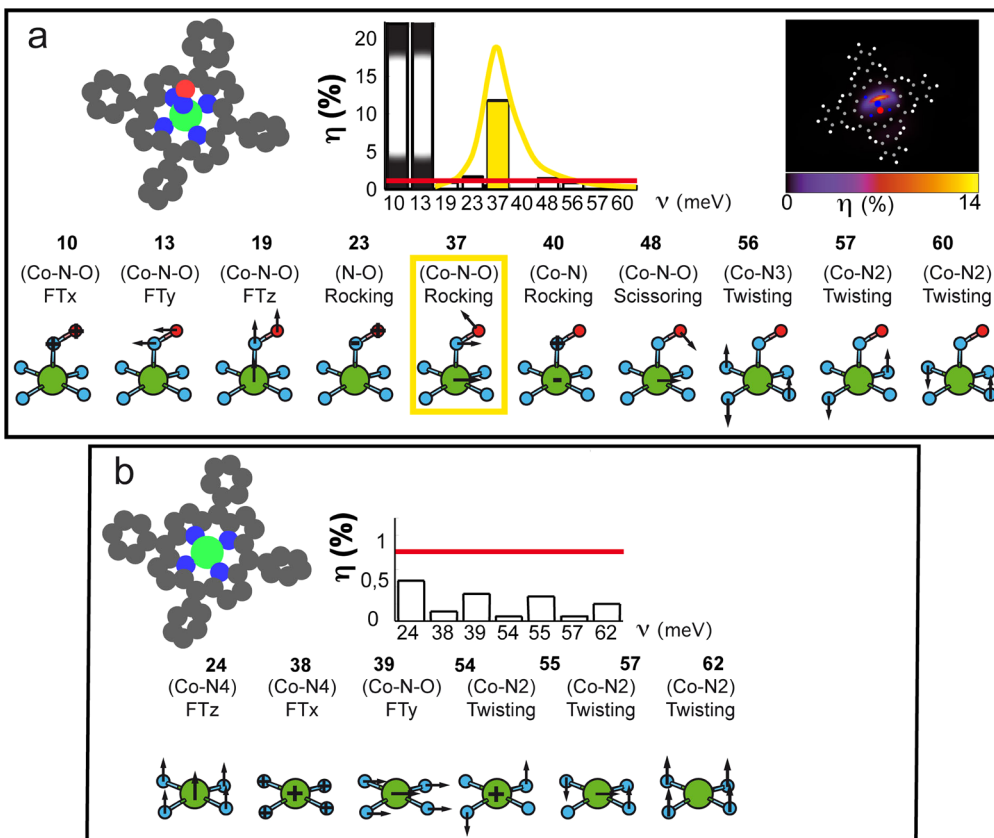


**Figure 7.** (a) (Left) Simulated IET spectra of NO-Co-TPP/Ag(111) above the center of the molecule;  $\eta$  is the inelastic fraction of electrons per vibration mode with a classification of the normal modes corresponding to the indicated vibration energies. The average experimental detection threshold of 1% is indicated by a horizontal red line. Three modes are active and highlighted in colors. The two low-energy modes marked in black Moiré are however discarded (see text). (Right) Simulated inelastic efficiency  $\eta$  over NO-Co-TPP/Ag(111) at a fixed  $V$  bias of 37 mV. The inelastic signal is spatially localized slightly off-center of the molecule. (b) Simulated IET spectra of bare Co-TPP/Ag(111) above the center of the molecule. None of the modes exceeds the experimental detection threshold of 1%. Energy values are in meV and correspond to vibrational calculations following model A in Figure 6. In the vibrational analysis, the directions of the lateral motions of participating atoms are indicated by arrows, correlated in size to the represented vibrational amplitudes. Movements directed out of the plane, toward or away from the reader, are displayed by + and - signs, respectively.

such method allows one to focus on NO-related signals. After excluding the 10 and 13 meV modes from our experiment–theory IETS comparison, we conclude that only the rocking mode at 37 meV, which involves the Co–N–O moiety, can be associated with the signature of the experiment. As such, our theoretical IETS simulations yield a theoretical spectrum with a single signal in very close agreement with the measured IET spectrum that displays only one narrow peak at 31 meV (Figure 3). It is interesting to note that other modes which have some contributions on the axial NO ligand (*i.e.*, the frequencies of 23 and 40 meV) turn silent in IETS.

## DISCUSSION

In the following discussion, we will show that our simulated spectra follow the selection rules of IETS, which have already been edicted on the response of small molecular adsorbates.<sup>25,29,31–38</sup> It is interesting to see whether the same arguments hold true for this significantly larger molecule, which is to date the largest interface that has ever been considered in IETS

simulations. The rule used to rationalize IETS in a straightforward way is the following: the vibration modes that yield large IET signals are those that can effectively modulate the electronic structure at the tunneling energy and affect the tunneling barrier. To understand IETS, it is therefore important to first determine the prevailing states for tunneling. For NO-Co-TPP, the frontier states—the HOMO and LUMO states sketched in Figure 5—involve a major contribution on the NO ligand. From an energetic point of view, both are eligible to contribute to the inelastic response. However, we also need to take the “tunneling barrier” criteria into account that has recently been revealed elsewhere.<sup>32</sup> This additional rule states that an electronic state survives in the spectroscopic tunneling if it offers a significant penetration into vacuum (dangling states). The HOMO state of NO-Co-TPP should therefore prevail over the LUMO, as it has large contributions on the Co, N, and O atoms that point into vacuum along the z-direction of their atomic orbitals (*e.g.*, out-of plane  $p_z$  and  $d_{z^2}$ ), while the LUMO lies in closer vicinity of the surface by having its

**TABLE 1. Calculated Energies of the Vibrational Modes of NO-Co-TPP in the Three Approximations Illustrated in Figure 6.<sup>a</sup>**

vibration (meV)	model A	model B	model C
(Co–N <sub>2</sub> ) twisting	60	59	80
(Co–N <sub>2</sub> ) twisting	57	56	80
(Co–N <sub>3</sub> ) twisting	56	55	80
(Co–N–O) scissoring	48	46	46
(Co–N) rocking	40	38	40
(Co–N–O) rocking	37	35	36
(N–O) rocking	23	21	20
(Co–N–O) FT <sub>z</sub>	19	19	14
(N–O) FT <sub>y</sub>	13	12	12
(N–O) FT <sub>x</sub>	10	7	5–8

<sup>a</sup>Only vibrations <60 meV are displayed as higher frequencies were not experimentally accessed with IETS.

contributions on the N and O atoms oriented parallel to it in the x- and y-directions (Figure 5). Hence, vibrations for which the movement of atoms remains in the normal plane like the rocking mode at 37 meV (indicated with arrows in Figure 7) will overlap with the electronic HOMO state and will consequently be active in IETS. On the other hand, vibrations for which the atoms move out of the plane (indicated with + and – signs in Figure 7) become inactive since they cannot overlap with the HOMO, as is the case for the two rocking modes at 40 and 23 meV.

Finally, we have also verified that employing the same simulation approach for the bare adsorbed porphyrin does not yield a result that could alternatively explain the singlet peak at 31 meV seen by experiment (Figure 3). In Figure 7 (bottom), we show the spectrum for its few vibrations below 60 meV, acquired at the same central position close to the Co atom. As becomes clear, none of these modes yield a detectable IET signal (all  $\eta$  efficiency values lie below 0.7%). However, one may question whether the prominent tunneling states for the bare porphyrin are also localized around the central region of the porphyrin in

order to validate the inner ring model used for the vibrations. Indeed, the two frontier states coherent with the two-fold symmetry of the STM contrast have strong contributions on the CoN<sub>4</sub> part (see Supporting Information). Hence our comparative IETS simulations unambiguously confirm the experimental findings that nonligated Co-TPP is inactive in IETS. In addition to our successful reproduction of the single measured IET signal at 31 meV for NO-Co-TPP, this permits illustration of the power of IETS simulations. IETS activity can thus be used as an indicator to sense and probe central, axial NO ligation on adsorbed metalloporphyrins.

## CONCLUSION

The combination of STM-IETS experiments and DFT calculations has proven to be a powerful tool for the identification of the IET activity of vibration modes of NO-ligated Co-TPP immobilized on a metallic substrate. The low binding energy of NO on Co-TPP hinders an extensive investigation of the electronic structure but, on the other hand, enables a controlled desorption, providing a distinct writing process on a molecular level. While the bare molecules display no IETS signal, the NO-ligated porphyrin exhibits a clear activity of a single vibration at an energy of 31 meV. Due to exhaustive IETS simulations, it was possible to assign the origin of this singlet peak acquired above the ligated species. Among many vibrations, one unique mode was found to be active, corresponding to the Co–N–O in-plane rocking mode. The IETS propensity rules that were verified earlier on much simpler molecules are extended to these complex species. In summary, this combined experimental and theoretical work succeeds for the first time in getting a fingerprint of the vibronic characteristic of NO-Co-TPP on a noble metal surface. In the future, it will be interesting to extend this methodology to other gaseous adducts on nanoconfined metalloporphyrins and related complex metal-organic units.

## EXPERIMENTAL SECTION

All experiments were performed in a commercial low-temperature STM based on the design described in ref 43, mounted in a custom-designed ultrahigh vacuum (UHV) chamber. The system base pressure was below  $2 \times 10^{-10}$  mbar, and all measurements were performed at 6 K to obtain high-resolution topographic and spectroscopic data. In the figure captions, V refers to the bias voltage applied to the sample. The STM images were taken in constant current mode and are processed by the WsXM program ([www.nanotec.es](http://www.nanotec.es)). The etched tungsten tip is prepared by argon bombardment and silver-coated by controlled dipping into the bare surface. The noble metal single-crystal surface was prepared by repeated cycles of argon sputtering (800 eV ion energy) and annealing to 725 K. Subsequently, Co-TPP was deposited by organic molecular beam epitaxy (OMBE) from a quartz crucible held at 625 K with a typical rate of less than one monolayer per hour. The porphyrins were synthesized by the Ruben group at Karlsruhe Institut für Technologie and degassed carefully, resulting in a background pressure in the mid- $10^{-10}$  mbar range during

evaporation. After depositing the porphyrin molecules at room temperature, the sample was cooled to 150 K for the dosing of nitrogen monoxide (NO, specified purity 99.8%) via a leak valve and subsequently transferred into the STM. Upon scanning, NO can be transferred to the STM tip, modifying the contrast and increasing the resolution.

In the presented experiments, we applied submonolayer coverages of the porphyrins and also kept the NO occupation of the porphyrins clearly below the saturation values in most experiments. This procedure results in clean metal patches, bare and decorated porphyrins on the same surface, and allows us to take measurements on all species with the very same tip under identical conditions. It should be noted that a full monolayer coverage as well as a full saturation of all porphyrins by the NO ligands can be achieved without difficulty, as shown in the controlled desorption experiments where initially all porphyrins were ligated (cf. Figure 2).

The inelastic ( $d^2/dV^2$ ) tunneling spectra are taken by using the lock-in technique. To improve the signal-to-noise ratio,

typically 20 individual spectra were recorded and averaged. This allowed us to restabilize the tip after every spectrum. We applied a lock-in frequency of 398 Hz with a bias modulation of  $\Delta V_{\text{rms}} = 3.5$  mV. The duration of a single spectrum was 60 s.

**Theoretical Section.** For the first-principles study, an ensemble of theoretical tools was employed within the framework of periodic density functional theory (DFT) using the Vienna Ab Initio Simulation Package (VASP).<sup>44,45</sup> For the consideration of electron–ion interactions, the projector-augmented wave (PAW) scheme<sup>46,47</sup> was used. The electronic one-particle wave functions were expanded in a plane wave basis set to an energy cutoff of 400 eV. The molecule–surface interactions for large  $\pi$ -orbital systems as the porphyrins in this study are mainly driven by van der Waals interactions, which may constitute a problematic case with the standard local and semilocal approximations to DFT due to the absence of dispersive forces. Here, we use the local density approximation (LDA)<sup>48</sup> to describe electron correlation and exchange interactions because it tends to approximately compensate for the lack of treating van der Waals interactions. The use of LDA is justified as it has previously yielded quantitative distances in related adsorbed  $\pi$ -orbital molecular systems.<sup>49–52</sup> Furthermore, non-spin-polarized calculations have been conducted for both bare Co-TPP and NO-Co-TPP adsorbed on the Ag(111) surface. Although pristine gas-phase Co-TPP initially has a molecular spin (one unpaired electron in the Co  $d_{z^2}$  orbital), this magnetism is suppressed when it adsorbs on a Cu surface by an electronic coupling between Co and the two nearest Cu neighbors.<sup>15</sup> We have carefully verified that the spin quenching holds similarly for a bare Co-TPP on a Ag surface. Additionally, when Co-TPP ligates the NO radical and forms the NO-Co-TPP complex, the molecular spin is cut but this time by the electronic coupling with the ligand. Hence, the adsorbed systems in this study remain closed shell.

The adsorptions of bare Co-TPP and NO-Co-TPP on the Ag(111) surface were modeled in the supercell approach, using repetitive slabs with a large  $p(11 \times 5\sqrt{3})$  surface periodicity. Each unit cell consisted of three atomic monolayers of silver onto which the molecules were absorbed, corresponding to over 400 atoms. The vacuum region between adjacent slabs is fixed to 15 Å. Integration over the first Brillouin zone was performed at the  $\Gamma$ -point with a Methfessel–Paxton smearing of 0.2 eV. The geometry optimizations of the adsorption complexes were carried out by relaxing the molecular degrees of freedom until atomic forces reached below a 0.05 eV/Å threshold. To reduce computational cost, the metal was kept rigid in its standard (111) slab configuration as defined by the theoretical lattice parameter calculated for bulk silver (4.02 Å).

The vibrations of these complex interfaces were evaluated by diagonalizing the dynamical matrix obtained from VASP while only taking some degrees of freedom of the adsorbate into account due to computational cost. Accordingly, only normal modes involving the central cobalt atom and nitrogen atoms composing the inner porphyrin ring were considered for Co-TPP, henceforth referred to as the ring approximation. As the coupling of low-energy vibrations to surface phonons was not accounted for in this study, possible IETS contributions from frustrated modes, particularly influenced by the latter, will be omitted from any subsequent analysis. In order to validate the obtained frequencies in the ring approximation for the entire NO-Co-TPP structure in the adsorbed phase, we performed equivalent vibration analyses of an all-included atom relaxation in the gas phase. Thus, we were able to quantify the possible deviations of our vibration approximation (see Table 1).

Finally, the IETS simulations of the porphyrins were carried out using a computational procedure based on a many-body extension<sup>53,54</sup> of the Tersoff–Hamann theory. Herein, the relative change in conductance  $\Delta\sigma/\sigma = \partial^2I/\partial V^2/\partial I/\partial V = \eta$  in the tunneling regime is obtained by considering the relative change in LDOS due to the perturbation of the wave function by the molecular vibration. Although the recorded IET spectrum strongly depends on the tip's position above the molecular species, only the center position has been selected here because this is the experimentally most relevant location.

*Conflict of Interest:* The authors declare no competing financial interest.

*Acknowledgment.* All authors thank the collaborative transnational grant in the ANR-DFG 2011 call (ANR-11-INTB-1014-01) for support. The initial experimental work was supported by the ERC Advanced Grant MolArt (No. 247299) and the Munich center for Advanced Photonics (MAP). W.A. acknowledges the Technische Universität München-Institute for Advanced Studies. S.R.B. and M.-L.B. are grateful for support from the FP7 Marie Curie Actions of the European Commission, via the Initial Training Network SMALL (MCITN-238804). S.R.B. and M.-L.B. also thank Emmanuel Quemener from the Centre Blaise Pascal (CBP) for code development and the Pole Scientifique de Modélisation Numérique (PSMN) for computational resources.

*Supporting Information Available:* Comparative raw IETS measured data and the comparative projected DOS onto some frontier MOs for the bare and the NO-ligated adsorbed Co-TPP. This material is available free of charge via the Internet at <http://pubs.acs.org>.

## REFERENCES AND NOTES

- Meunier, B. Metalloporphyrins as Versatile Catalysts for Oxidation Reactions and Oxidative DNA Cleavage. *Chem. Rev.* **1992**, *92*, 1411–1456.
- Ghosh, A. Metalloporphyrin–NO Bonding: Building Bridges with Organometallic Chemistry. *Acc. Chem. Res.* **2005**, *38*, 943–954.
- Wyer, J. A.; Brøndsted Nielsen, S. Absorption by Isolated Ferric Heme Nitrosyl Cations in Vacuo. *Angew. Chem., Int. Ed.* **2012**, *51*, 10256–10260.
- Spiro, T. G.; Soldatova, A. V.; Balakrishnan, G. CO, NO and O<sub>2</sub> as Vibrational Probes of Heme Protein Interactions. *Coord. Chem. Rev.* **2013**, *257*, 511–527.
- Lanucara, F.; Chiavarino, B.; Crestoni, M. E.; Scuderi, D.; Sinha, R. K.; Maître, P.; Fornarini, S. Naked Five-Coordinate FeIII(NO) Porphyrin Complexes: Vibrational and Reactivity Features. *Inorg. Chem.* **2011**, *50*, 4445–4452.
- Domke, K. F.; Pettinger, B. *In Situ* Discrimination between Axially Complexed and Ligand-Free Cobalt Porphyrin on Au(111) with Tip-Enhanced Raman Spectroscopy. *ChemPhysChem* **2009**, *10*, 1794–1798.
- Scheidt, W. R.; Ellison, M. K. The Synthetic and Structural Chemistry of Heme Derivatives with Nitric Oxide Ligands. *Acc. Chem. Res.* **1999**, *32*, 350–359.
- Groombridge, C. J.; Larkworthy, L. F.; Mason, J. Swinging of the Bent Nitrosyl Ligand in [Co(<sup>15</sup>NO)(TPP)]: A Solid-State Motion Detected by <sup>15</sup>N CPMAS NMR Spectroscopy. *Inorg. Chem.* **1993**, *32*, 379–380.
- Grande, L. M.; Noll, B. C.; Oliver, A. G.; Scheidt, W. R. Dynamics of NO Motion in Solid-State [Co(tetraphenylporphinate)(NO)]. *Inorg. Chem.* **2010**, *49*, 6552–6557.
- Flechtnar, K.; Kretschmann, A.; Steinrück, H.-P.; Gottfried, J. M. NO-Induced Reversible Switching of the Electronic Interaction between a Porphyrin-Coordinated Cobalt Ion and a Silver Surface. *J. Am. Chem. Soc.* **2007**, *129*, 12110–12111.
- Seufert, K.; Auwärter, W.; Barth, J. V. Discriminative Response of Surface-Confining Metalloporphyrin Molecules to Carbon and Nitrogen Monoxide. *J. Am. Chem. Soc.* **2010**, *132*, 18141–18146.
- Lehnert, N.; Sage, J. T.; Silvernail, N.; Scheidt, W. R.; Alp, E. E.; Sturhahn, W.; Zhao, J. Oriented Single-Crystal Nuclear Resonance Vibrational Spectroscopy of [Fe(TPP)(MI)(NO)]: Quantitative Assessment of the Trans Effect of NO. *Inorg. Chem.* **2010**, *49*, 7197–7215.
- Scheidt, W. R.; Hoard, J. L. Stereochemistry of Low-Spin Cobalt Porphyrins. I. Structure and Bonding in a Nitrosyl-cobalt Porphyrin and their Bearing on One Rational Model for the Oxygenated Protoheme. *J. Am. Chem. Soc.* **1973**, *95*, 8281–8288.
- Auwärter, W.; Seufert, K.; Klappenberger, F.; Reichert, J.; Weber-Bargioni, A.; Verdini, A.; Cvetko, D.; Dell'Angela, M.; Floreano, L.; Cossaro, A.; et al. Site-Specific Electronic and

- Geometric Interface Structure of Co-Tetraphenyl-Porphyrin Layers on Ag(111). *Phys. Rev. B* **2010**, *81*, 245403.
15. Seufert, K.; Bocquet, M.-L.; Auwärter, W.; Weber-Bargioni, A.; Reichert, J.; Lorente, N.; Barth, J. V. *cis*-Dicarbonyl Binding at Cobalt and Iron Porphyrins with Saddle-Shape Conformation. *Nat. Chem.* **2011**, *3*, 114–119.
  16. Diller, K.; Klappenberger, F.; Marschall, M.; Hermann, K.; Nefedov, A.; Wöll, C.; Barth, J. V. Self-Metalation of 2H-Tetraphenylporphyrin on Cu(111): An X-ray Spectroscopy Study. *J. Chem. Phys.* **2012**, *136*, 014705.
  17. Lukasczyk, T.; Flechtner, K.; Merte, L. R.; Jux, N.; Maier, F.; Gottfried, J. M.; Steinrück, H.-P. Interaction of Cobalt(II) Tetraarylporphyrins with a Ag(111) Surface Studied with Photoelectron Spectroscopy. *J. Phys. Chem. C* **2007**, *111*, 3090–3098.
  18. Wäckerlin, C.; Chylarecka, D.; Kleibert, A.; Müller, K.; Iacovita, C.; Nolting, F.; Jung, T. A.; Ballav, N. Controlling Spins in Adsorbed Molecules by a Chemical Switch. *Nat. Commun.* **2010**, *1*, 61.
  19. Stipe, B. C.; Rezaei, M. A.; Ho, W. Single-Molecule Vibrational Spectroscopy and Microscopy. *Science* **1998**, *280*, 1732–1735.
  20. Ho, W. Single-Molecule Chemistry. *J. Chem. Phys.* **2002**, *117*, 11033–11061.
  21. Ueba, H. Motions and Reactions of Single Adsorbed Molecules Induced by Vibrational Excitation with STM. *Surf. Rev. Lett.* **2003**, *10*, 771–796.
  22. Lorente, N.; Rurali, R.; Tang, H. Single-Molecule Manipulation and Chemistry with the STM. *J. Phys.: Condens. Matter* **2005**, *17*, S1049.
  23. Komeda, T. Chemical Identification and Manipulation of Molecules by Vibrational Excitation via Inelastic Tunneling Process with Scanning Tunneling Microscopy. *Prog. Surf. Sci.* **2005**, *78*, 41–85.
  24. Franke, K. J.; Schulze, G.; Pascual, J. I. Excitation of Jahn–Teller Active Modes during Electron Transport through Single C<sub>60</sub> Molecules on Metal Surfaces. *J. Phys. Chem. Lett.* **2010**, *1*, 500–504.
  25. Bocquet, M.-L.; Lesnard, H.; Lorente, N. Inelastic Spectroscopy Identification of STM-Induced Benzene Dehydrogenation. *Phys. Rev. Lett.* **2006**, *96*, 096101.
  26. Gaudioso, J.; Lee, H. J.; Ho, W. Vibrational Analysis of Single Molecule Chemistry: Ethylene Dehydrogenation on Ni(110). *J. Am. Chem. Soc.* **1999**, *121*, 8479–8485.
  27. Parschau, M.; Rieder, K.-H.; Hug, H. J.; Ernst, K.-H. Single-Molecule Chemistry and Analysis: Mode-Specific Dehydrogenation of Adsorbed Propene by Inelastic Electron Tunneling. *J. Am. Chem. Soc.* **2011**, *133*, 5689–5691.
  28. Fock, J.; Sørensen, J. K.; Lörtscher, E.; Vosch, T.; Martin, C. A.; Riel, H.; Kilså, K.; Bjørnholm, T.; van der Zant, H. A Statistical Approach to Inelastic Electron Tunneling Spectroscopy on Fullerene-Terminated Molecules. *Phys. Chem. Chem. Phys.* **2011**, *13*, 14325–14332.
  29. Burema, S. R.; Bocquet, M.-L. Sensitizers in Inelastic Electron Tunneling Spectroscopy: A First-Principles Study of Functional Aromatics on Cu(111). *Nanotechnology* **2012**, *23*, 315702.
  30. Gaudioso, J.; Ho, W. Single-Molecule Vibrations, Conformational Changes, and Electronic Conductivity of Five-Membered Heterocycles. *J. Am. Chem. Soc.* **2001**, *123*, 10095–10098.
  31. Burema, S. R.; Bocquet, M.-L. Resonance Charges To Encode Selection Rules in Inelastic Electron Tunneling Spectroscopy. *J. Phys. Chem. Lett.* **2012**, *3*, 3007–3011.
  32. Burema, S. R.; Lorente, N.; Bocquet, M.-L. A Theoretical Rationalization of a Total Inelastic Electron Tunneling Spectrum: The Comparative Cases of Formate and Benzoate on Cu(111). *J. Chem. Phys.* **2012**, *136*, 244507.
  33. Lorente, N.; Persson, M.; Lauhon, L. J.; Ho, W. Symmetry Selection Rules for vibrationally Inelastic Tunneling. *Phys. Rev. Lett.* **2001**, *86*, 2593–2596.
  34. Troisi, A.; Ratner, M. A. Molecular Transport Junctions: Propensity Rules for Inelastic Electron Tunneling Spectra. *Nano Lett.* **2006**, *6*, 1784–1788.
  35. Paulsson, M.; Frederiksen, T.; Ueba, H.; Lorente, N.; Brandbyge, M. Unified Description of Inelastic Propensity Rules for Electron Transport through Nanoscale Junctions. *Phys. Rev. Lett.* **2008**, *100*, 226604.
  36. Bocquet, M.-L.; Lorente, N. Probing the Proton Location in a Water Bilayer on Pd (111) by Inelastic Spectroscopy Simulations. *J. Chem. Phys.* **2009**, *130*, 124702.
  37. Lesnard, H.; Bocquet, M.-L.; Lorente, N. Dehydrogenation of Aromatic Molecules under a Scanning Tunneling Microscope: Pathways and Inelastic Spectroscopy Simulations. *J. Am. Chem. Soc.* **2007**, *129*, 4298–4305.
  38. Alducin, M.; Sánchez-Portal, D.; Arnau, A.; Lorente, N. Mixed-Valency Signature in Vibrational Inelastic Electron Tunneling Spectroscopy. *Phys. Rev. Lett.* **2010**, *104*, 136101.
  39. Hieringer, W.; Flechtner, K.; Kretschmann, A.; Seufert, K.; Auwärter, W.; Barth, J. V.; Görling, A.; Steinrück, H.-P.; Gottfried, J. M. The Surface Trans Effect: Influence of Axial Ligands on the Surface Chemical Bonds of Adsorbed Metalloporphyrins. *J. Am. Chem. Soc.* **2011**, *133*, 6206–6222.
  40. Alemani, M.; Peters, M. V.; Hecht, S.; Rieder, K.-H.; Moresco, F.; Grill, L. Electric Field-Induced Isomerization of Azobenzene by STM. *J. Am. Chem. Soc.* **2006**, *128*, 14446–14447.
  41. Sloan, P. A.; Sakulsermsuk, S.; Palmer, R. E. Nonlocal Desorption of Chlorobenzene Molecules from the Si(111)-(7 × 7) Surface by Charge Injection from the Tip of a Scanning Tunneling Microscope: Remote Control of Atomic Manipulation. *Phys. Rev. Lett.* **2010**, *105*, 048301.
  42. Morgenstern, K. On the Interpretation of IETS Spectra of a Small Organic Molecule. *J. Phys.: Condens. Matter* **2011**, *23*, 484007.
  43. Meyer, G. A Simple Low-Temperature Ultrahigh-Vacuum Scanning Tunneling Microscope Capable of Atomic Manipulation. *Rev. Sci. Instrum.* **1996**, *67*, 2960–2965.
  44. Kresse, G.; Furthmüller, J. Efficiency of *Ab-Initio* Total Energy Calculations for Metals and Semiconductors Using a Plane-Wave Basis Set. *Comput. Mater. Sci.* **1996**, *6*, 15–50.
  45. Kresse, G.; Furthmüller, J. Efficient Iterative Schemes for *Ab-Initio* Total-Energy Calculations Using a Plane-Wave Basis Set. *Phys. Rev. B* **1996**, *54*, 11169–11186.
  46. Kresse, G.; Joubert, D. From Ultrasoft Pseudopotentials to the Projector Augmented-Wave Method. *Phys. Rev. B* **1999**, *59*, 1758–1775.
  47. Blöchl, P. E. Projector Augmented-Wave Method. *Phys. Rev. B* **1994**, *50*, 17953–17979.
  48. Perdew, J. P.; Zunger, A. Self-Interaction Correction to Density-Functional Approximations for Many-Electron Systems. *Phys. Rev. B* **1981**, *23*, 5048–5079.
  49. Vladimirova, M.; Trimarchi, G.; Baldereschi, A.; Weckesser, J.; Kern, K.; Barth, J.; De Vita, A. Substrate-Induced Supramolecular Ordering of Functional Molecules: Theoretical Modelling and STM Investigation of the PEBA/Ag(111) System. *Acta Mater.* **2004**, *52*, 1589–1595.
  50. Rohlfing, M.; Temirov, R.; Tautz, F. S. Adsorption Structure and Scanning Tunneling Data of a Prototype Organic–Inorganic Interface: PTCDA on Ag(111). *Phys. Rev. B* **2007**, *76*, 115421.
  51. Klappenberger, F.; Cañas-Ventura, M. E.; Clair, S.; Pons, S.; Schlickum, U.; Qu, Z.-R.; Brune, H.; Kern, K.; Strunkus, T.; Wöll, C.; et al. Conformational Adaptation in Supramolecular Assembly on Surfaces. *ChemPhysChem* **2007**, *8*, 1782–1786.
  52. Franke, K. J.; Schulze, G.; Henningsen, N.; Fernández-Torrente, I.; Pascual, J. I.; Zarwell, S.; Rück-Braun, K.; Cobian, M.; Lorente, N. Reducing the Molecule–Substrate Coupling in C<sub>60</sub>-Based Nanostructures by Molecular Interactions. *Phys. Rev. Lett.* **2008**, *100*, 036807.
  53. Lorente, N.; Persson, M. Theory of Single Molecule Vibrational Spectroscopy and Microscopy. *Phys. Rev. Lett.* **2000**, *85*, 2997–3000.
  54. Lorente, N. Mode Excitation Induced by the Scanning Tunnelling Microscope. *Appl. Phys. A: Mater. Sci. Process.* **2004**, *78*, 799–806.